Autophagy 8:8, 1175–1184; August 2012; © 2012 Landes Bioscience

Immunohistochemical detection of cytoplasmic LC3 puncta in human cancer specimens

Sylvain Ladoire,[1,2,3,†] Kariman Chaba,[1,2,†] Isabelle Martins,[2,4,5] Abdul Qader Sukkurwala,[2,4,5] Sandy Adjemian,[2,4,5] Mickaël Michaud,[2,4,5] Vichnou Poirier-Colame,[1,2] Felipe Andreiuolo,[2,6] Lorenzo Galluzzi,[2,7] Eileen White,[8,9] Mathias Rosenfeldt,[10] Kevin M. Ryan,[10] Laurence Zitvogel[1,2,5,11] and Guido Kroemer[2,4,7,12,13,*]

[1]INSERM; U1015; Villejuif, France; [2]Institut Gustave Roussy; Villejuif, France; [3]Department of Medical Oncology; Centre Georges François Leclerc; Dijon, France; [4]INSERM; U848; Villejuif, France; [5]Faculté de Médecine; Université Paris Sud-XI; Le Kremlin Bicêtre; Paris, France; [6]Department of Pathology; Institut Gustave Roussy; Villejuif, France; [7]Sorbonne Paris Cité; Université Paris Descartes; Paris, France; [8]The Cancer Institute of New Jersey; New Brunswick, NJ USA; [9]Department of Molecular Biology and Biochemistry; Rutgers University; Piscataway, NJ USA; [10]Tumour Cell Death Laboratory; Beatson Institute for Cancer Research; Glasgow, UK; [11]Center of Clinical Investigations in Biotherapies of Cancer (CICBT); Villejuif, France; [12]Centre de Recherche des Cordeliers; Paris, France; [13]Pôle de Biologie; Hôpital Européen Georges Pompidou; Paris, France

[†]These authors contributed equally to this work.

Keywords: autophagosomes, CT26, immunohistochemistry, lysosomes, macroautophagy, MCA205

Autophagy is an evolutionarily conserved catabolic process that involves the entrapment of cytoplasmic components within characteristic vesicles for their delivery to and degradation within lysosomes. Alterations in autophagic signaling are found in several human diseases including cancer. Here, we describe a validated immunohistochemical protocol for the detection of LC3 puncta in human formalin-fixed, paraffin-embedded cancer specimens that can also be applied to mouse tissues. In response to systemic chemotherapy, autophagy-competent mouse tumors exhibited LC3 puncta, which did not appear in mouse cancers that had been rendered autophagy-deficient by the knockdown of Atg5 or Atg7. As compared with normal tissues, LC3 staining was moderately to highly elevated in the large majority of human cancers studied, albeit tumors of the same histological type tended to be highly heterogeneous in the number and intensity of LC3 puncta per cell. Moreover, tumor-infiltrating immune cells often were highly positive for LC3. Altogether, this protocol for LC3 staining appears suitable for the specific detection of LC3 puncta in human specimens, including tissue microarrays. We surmise that this technique can be employed for retrospective or prospective studies involving large series of human tumor samples.

Introduction

Although autophagy was initially described in the 1960s by De Duve,[1] this phenomenon received little attention until recently, when a better comprehension of the genes involved in the autophagic process, and improved methods to detect it, contributed to an exponential increase in autophagy research.[2]

Autophagy is a self-catabolic process that maintains intracellular homeostasis and prolongs cell survival under stress by allowing for the lysosomal degradation of damaged cytoplasmic constituents and for recycling of amino acids and energy.[3] Autophagy is orchestrated by a number of highly conserved AuTophaGy-related genes (ATGs).[4,5] In mammalian cells, double-membraned autophagosomes develop in a multistep process from a precursor structure called a phagophore. Autophagosomes subsequently fuse with lysosomes to form a single-membraned vesicle called an autolysosome.[6] Alterations in the biochemical nature and subcellular localization of Atg8/LC3 (microtubule-associated protein 1 light chain 3) correlate with autophagy and hence are used as surrogate markers for its quantification.[7,8] Newly synthesized LC3 is immediately cleaved at its C-terminus by the protease ATG4 to generate the cytoplasmic form LC3-I. Under normal conditions, when autophagy is off, LC3-I distributes diffusely throughout the cytoplasm. However, upon induction of autophagy, LC3 is conjugated to the lipid phosphatidylethanolamine by ATG7 and ATG3, resulting in its redistribution to autophagosomal membranes.[9] This form of LC3, which is called LC3-II, is recruited via its lipid moiety to the inner and outer surfaces of autophagosome membranes, hence forming LC3-decorated autophagic puncta.

Over the past decade, many studies have shown that autophagy is critically important for the survival, activation and differentiation of multiple cell types, as well as for the pathogenesis of several human diseases. Thus, deficient or excessive autophagy has been reported to occur in, and to contribute to, healthy and pathological aging, degenerative diseases of many organs, inflammation, infectious disease, and cancer.[10] During malignant transformation, as well as in response to cancer therapy, autophagy reportedly promotes either cell survival or death.[11]

*Correspondence to: Guido Kroemer; Email: kroemer@orange.fr
Submitted: 01/05/12; Revised: 04/11/12; Accepted: 04/11/12
http://dx.doi.org/10.4161/auto.20353

Proper detection methods are therefore critical for assessing the pathophysiological impact of autophagy. So far, autophagy has mainly been studied in cultured cells, by following the redistribution of GFP-LC3 fusion proteins to autophagic puncta by fluorescence microscopy, by assessing the conversion of LC3-I to LC3-II by immunoblotting, or by the quantification of double-membraned autophagosomes using transmission electron microscopy.[7,12] A critical limitation for the in vivo detection of autophagosomes is the lack of convenient immunohistochemical methods applicable to common formalin-fixed, paraffin-embedded tissues. Here, we describe a protocol for detecting autophagic puncta in such tissues, using an antibody that recognizes both the soluble (LC3-I) and the membrane-bound form (LC3-II) of LC3. This method is applicable to mouse tissues as well as to an array of human formalin-fixed, paraffin-embedded cancer specimens.

Results

Immunohistochemistry of cancer cell lines. The reactivity of the anti-LC3 antibody was first tested on mouse colon carcinoma CT26 cells that were either maintained in control conditions or stimulated to undergo autophagy by two distinct means (nutrient-free medium and 10 μM rapamycin) for up to 8 h. To obtain insights into the autophagic flux, these treatments were all performed both in the absence and in the presence of the lysosomal inhibitor bafilomycin A_1 (BafA1). At the end of the incubation, CT26 cells were washed, centrifuged, and the cellular sediment was embedded in paraffin to generate 4 μm-thick sections. The number of cytoplasmic $LC3^+$ puncta/cell, indicative of the conversion of LC3-I into LC3-II, increased in a time-dependent manner following the shift to nutrient-free medium as well as in response to rapamycin (but not in control conditions) (**Fig. 1A and B**). The presence of $BafA_1$ further increased the amount of cytoplasmic $LC3^+$ dots (**Fig. 1A and B**), demonstrating that our method can provide an appropriate overlook on the autophagic flux. To compare our technique to conventional approaches for the detection of autophagy, we took advantage of CT26 cells stably expressing a GFP-LC3 chimera. In response to pro-autophagic triggers, these cells exhibit green cytoplasmic dots that can be easily quantified by confocal fluorescence microscopy.[7] The data sets obtained by immunohistochemistry (**Fig. 1B**) and fluorescence microscopy (**Fig. S2A and S2B**) correlated with each other with an $R^2 > 0.87$, suggesting that the performance of our immunohistochemical method is non-inferior to that of widely accepted techniques for monitoring autophagy. Of note, when the LC3-targeting antibody was replaced by an isotype matched non-specific IgG, both control and autophagic cells remained unstained, confirming the specificity of our immunohistochemical approach (**Fig. S1**).

To provide additional insights into the selectivity of our method, we took advantage of CT26 cells stably expressing shRNAs against the essential autophagic regulators Atg5 and Atg7 (**Fig. S2C**). At odds with their control counterparts (SCR cells), $Atg5^{KD}$ and $Atg7^{KD}$ cells are unable to convert LC3-I into LC3-II in response to pro-autophagic triggers,[13] including rapamycin and mitoxantrone (MTX) (**Fig. S2C**). In line with this notion, SCR, but not $Atg5^{KD}$ and $Atg7^{KD}$, CT26 cells responded to rapamycin by accumulating cytoplasmic $LC3^+$ dots, which could be detected with comparable results by immunohistochemistry (**Fig. 1C and D**) or indirect immunofluorescence microscopy (**Fig. S2D and S2E**).

Immunohistochemistry of mice tumors. To validate LC3 as a potential biomarker for in situ autophagosome formation in cancer cells, we inoculated mice SCR, $Atg5^{KD}$ or $Atg7^{KD}$ colon carcinoma CT26 or fibrosarcoma MCA205 tumor cells. Mice were then either left untreated or treated with MTX. In contrast to autophagy-competent cancers, LC3 puncta were not observed in tumors derived from $Atg5^{KD}$ or $Atg7^{KD}$ cells (**Fig. 2A and B**). These results suggest that our protocol does allow for the accurate monitoring of autophagy in preclinical murine models.

Immunohistochemistry of tissue microarrays derived from normal and neoplastic human tissues. To evaluate the validity of our approach on several, distinct human tissues, we took advantage of tissue microarrays containing 18 different types of nonmalignant tissues, as well as invasive or metastatic specimens from 31 different types of human cancer. This tissue microarray was processed for the immunohistochemical detection of LC3, and the intensity and subcellular distribution of the staining was assessed by a trained histologist (SL). Similar to cellular samples (**Fig. S1**), tissue sections remained unstained when the anti-LC3 antibody was substituted by an isotype-matched nonspecific IgG, further corroborating the specificity of our immunohistochemical method (**Fig. S3**).

Staining often (but not always) was rather homogenous across tissue sections. Except for cerebral and placental tissue, LC3 staining of noncancerous sections was generally weak as compared with histologically matched tumor specimens (**Figs. 3, 4 and 5**). However, LC3 puncta were never seen in nonmalignant tissues, with the notable exception of a few neuronal cell bodies present in the cerebral cortex or hippocampus (**Fig. 3G and H**). The LC3-specific signal was predominantly localized in the cytoplasm, and

Figure 1 (See opposite page). LC3 staining in cultured cells. (A and B) Mouse colon carcinoma CT26 cells were left untreated (Co), treated with 10 μM rapamycin (Rapa) or maintained in nutrient-free (NF) conditions, in the absence or in the presence of 1 μg/mL bafilomycin A_1 (BafA1) for the indicated time. (C and D) Alternatively, CT26 cells expressing a control shRNA (SCR cells) as well as cells expressing Atg5- ($Atg5^{KD}$) or Atg7-specific ($Atg7^{KD}$) shRNAs were maintained in control conditions or administered with 1 μg/mL Rapa for 8 h. After stimulation, cells were processed for the immunohistochemical detection of LC3. Representative images (A and C) and quantitative data (B and D) are shown. Scale bars: 10 or 30 μm, as indicated. In (B and D), columns depict the number of $LC3^+$ cytoplasmic dots/cell. Data are presented as means ± SEM (n = 3; $^*p < 0.05$, $^{**}p < 0.001$, Student's t-test, compared with WT or SCR cells maintained in control conditions; $^{\#}p < 0.05$, $^{\#\#}p < 0.001$, Student's t-test, as compared with WT or SCR cells treated with the same autophagic trigger in the absence of BafA1).

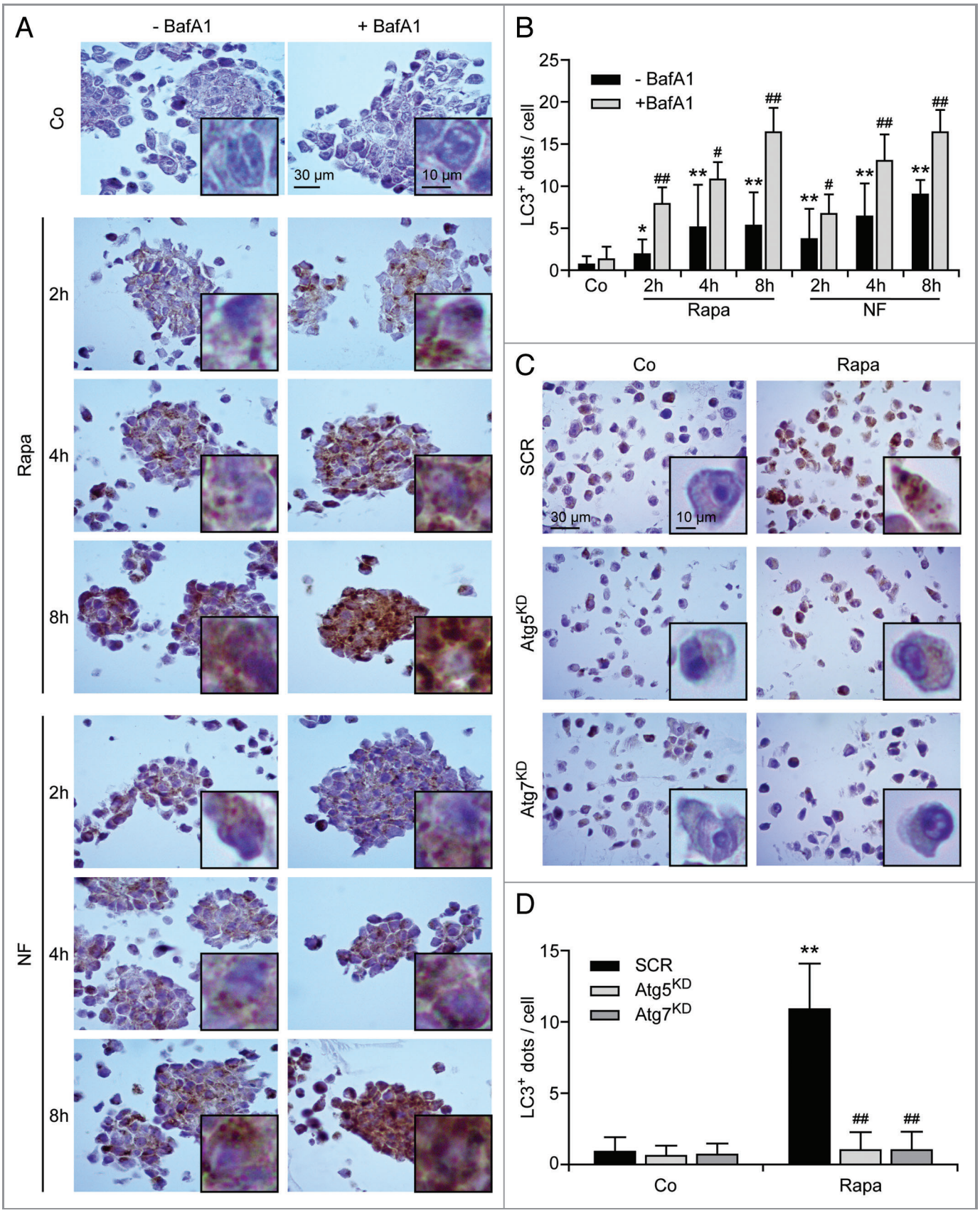

Figure 1. For figure legend, see page 1176.

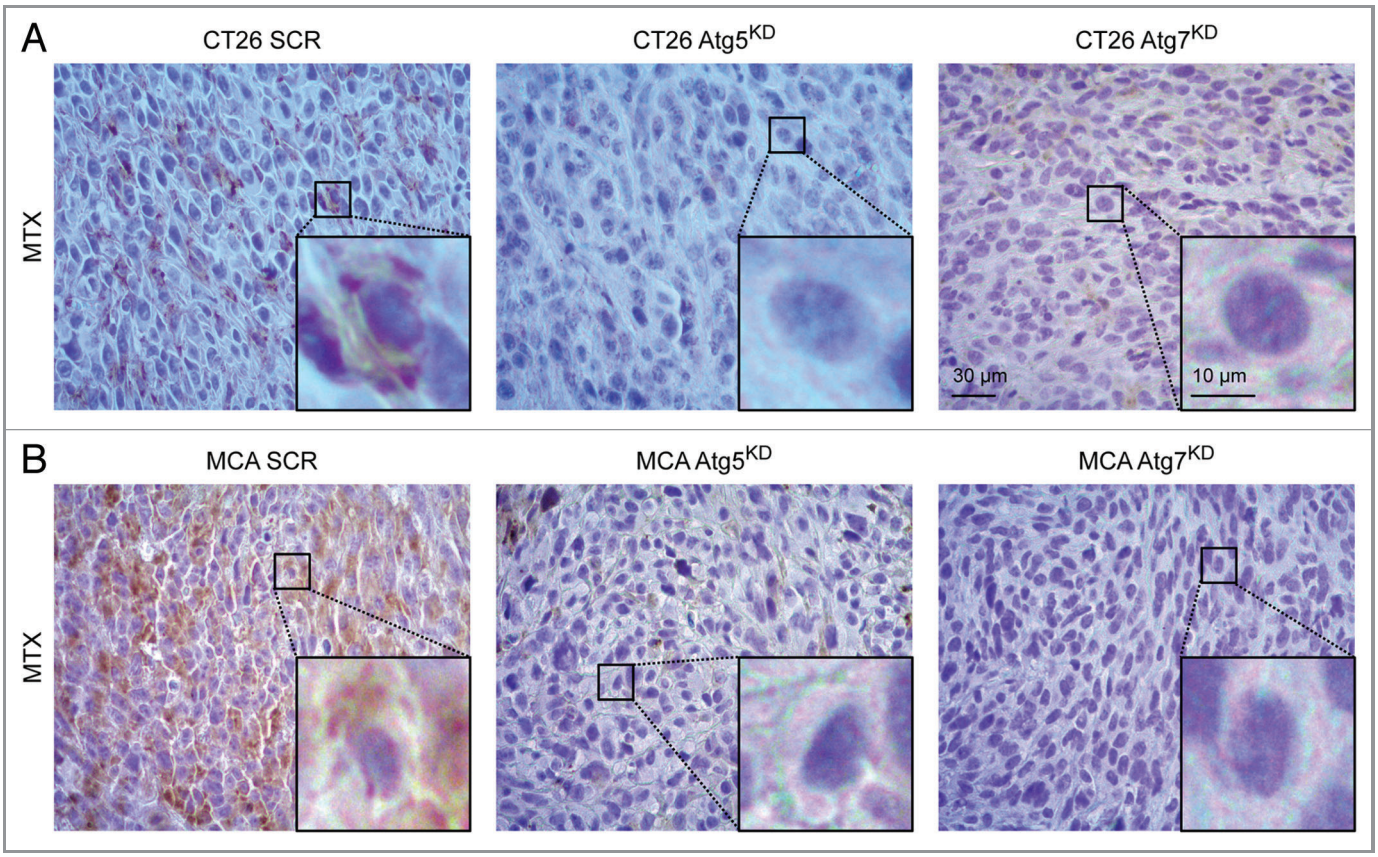

Figure 2. LC3 staining in situ, in preclinical tumor models. (A and B) Murine colon carcinoma CT26 (A, left panel) or murine fibrosarcoma MCA205 cells (B, left panel) expressing a control shRNA (SCR cells), as well as their Atg5- (middle panels) or Atg7-knockdown (right panels) derivatives, were allowed to grow in vivo in syngenic mice until tumors reached a surface area of 40–80 mm^2. Mice were then treated with systemic mitoxantrone (MTX) for 2 d, followed by tumor recovery and processing for the immunohistochemical detection of LC3. Representative images are shown. Scale bars: 10 or 30 μm, as indicated.

appeared to be weak in 37% and strong (though without LC3 puncta) in 47% of nonmalignant tissues (**Table S1**).

In tumor samples, the presence of LC3 puncta was observed in the context of strong cytoplasmic staining. LC3 staining was strong without (29% of cases) or with (45% of cases) LC3 puncta in the large majority of human tumors. Of note, although LC3 puncta could be detected in the majority of tumor samples (**Fig. 6A and C**; **Fig. S4A and S4B**), a significant fraction of tumors (26%) only exhibited a weak LC3 staining, in the absence of detectable LC3 puncta (**Fig. 4B, D, F and H**; **Fig. 6B and D**; **Fig. S4C and Fig. S5G**). Moreover, specimens from histologically similar tumors (representative results for three different lung adenocarcinomas and three different breast adenocarcinomas are shown in **Fig. 4A–C and 4D–F**, respectively) exhibited a heterogeneous intensity of staining. Frequently, immune cells that infiltrated normal or cancer tissues exhibited a strong cytoplasmic LC3 staining (**Fig. S6**).

Immunohistochemistry of formalin-fixed, paraffin-embedded breast carcinoma specimens. In a further attempt to demonstrate the applicability of our staining procedure, tumor blocks from 95 patients treated for localized breast cancer were retrieved from the archives of the Department of Pathology of the Institut Gustave Roussy (Villejuif, France), and 4 μm-thick slides were stained for the visualization of LC3. LC3 was detected in most, if not all, the 95 specimens, at least in some stromal elements, though with distinct staining patterns in cancer cells. Twenty-three (24%) cancers exhibited negative or weak staining (**Fig. 7A**). Forty-one (43%) cancers exhibited significant diffuse cytoplasmic staining without puncta (**Fig. 7B**). Finally, in 31 tumors (33%) LC3 puncta were detectable in the majority of the tumor cells (**Fig. 7C and D**). Importantly, normal breast tissues failed to stain positively for LC3 (0.81 ± 0.17 $LC3^+$ cytoplasmic dots/cell, as quantified among 15–20 cells in n = 5 independent samples), contrasting with adjacent cancer cells that often exhibited a diffuse or punctate LC3 staining pattern (in the latter case, 7.89 ± 0.64 $LC3^+$ cytoplasmic dots/cell, as quantified among 15–20 cells in n = 5 independent samples) (**Fig. 7D**).

Discussion

The assessment of autophagy in tissues is mostly based on the detection of autophagosomes using transmission electron microscopy (TEM),[14,15] a technique that is laborious and requires considerable expertise, especially at the level of image analysis.

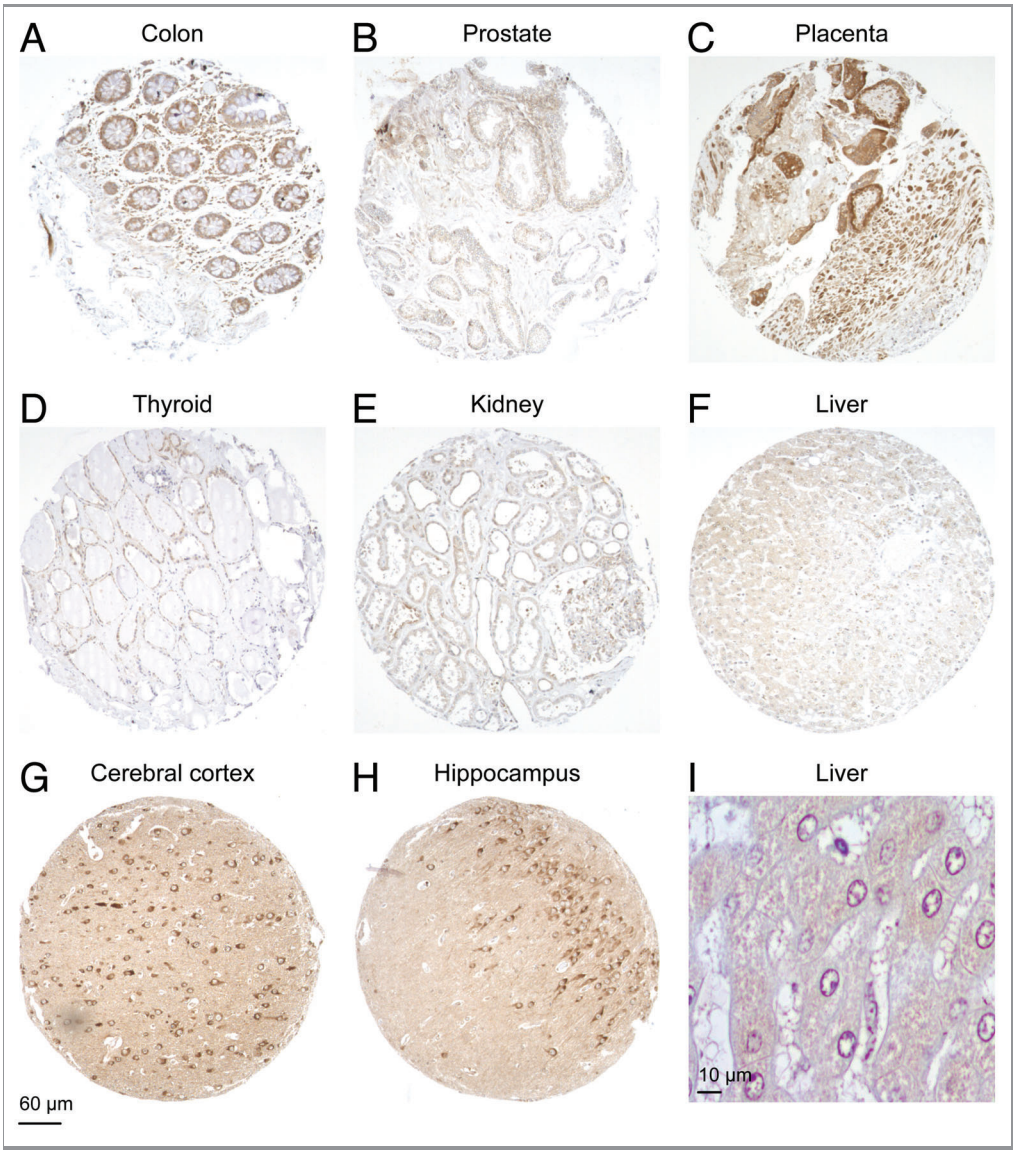

Figure 3. Representative LC3 staining patterns in nonmalignant tissues. Tissue microarrays encompassing distinct normal tissues were stained for the immunohistochemical detection of LC3, as detailed in Materials and Methods. Representative images are reported: (A) colon, (B) prostate, (C) placenta, (D) thyroid gland, (E) kidney, (F) liver, (G) cerebral cortex, (H) hippocampus and (I) detail of the weak diffuse cytoplasmic staining observed in normal hepatocytes. Scale bar: 10 or 60 μm, as indicated.

Thus, various cytoplasmic structures have been misidentified as autophagic vacuoles in the recent literature, most likely because of the lack of morphological expertise to correctly interpret TEM images.[7] Moreover, artifacts can be generated during fixation and staining procedures, and other organelles such as the endoplasmic reticulum can swell in stressed or dying cells, leading to an autophagy-unrelated cytoplasmic vacuolization.[7] Immunoelectron microscopy using antibodies against autophagosomal proteins can improve the detection of autophagosomes,[8,16] but this method is particularly cumbersome. In preclinical models, quantification of GFP-LC3 puncta by fluorescence microscopy in GFP-LC3-transfected cells and the immunoblotting-based detection of the conversion of LC3-I to LC3-II have been widely used.[2,7,17,18] However, despite numerous preclinical studies suggesting that the pharmacological modulation of autophagy might be useful in cancer treatment,[13,19-22] the clinical implications of elevated or suppressed autophagy in human malignancies remains largely unknown. Hence, a convenient method for detecting endogenous LC3 puncta that is applicable to paraffin-embedded human tissues may constitute a decisive advantage.

In mammals, LC3 is expressed as 3 isoforms: A, B and C. Here, we used an antibody that was generated against the N-terminus of human LC3B to investigate the expression and subcellular localization of LC3B in human or mouse cancer cells. We gave preference to LC3B due to its broad tissue specificity and its previous characterization as an autophagosome marker in cancer.[7,23,24] Nonetheless, to obtain a complete picture of the formation of autophagic vacuoles in tissues, it might be important

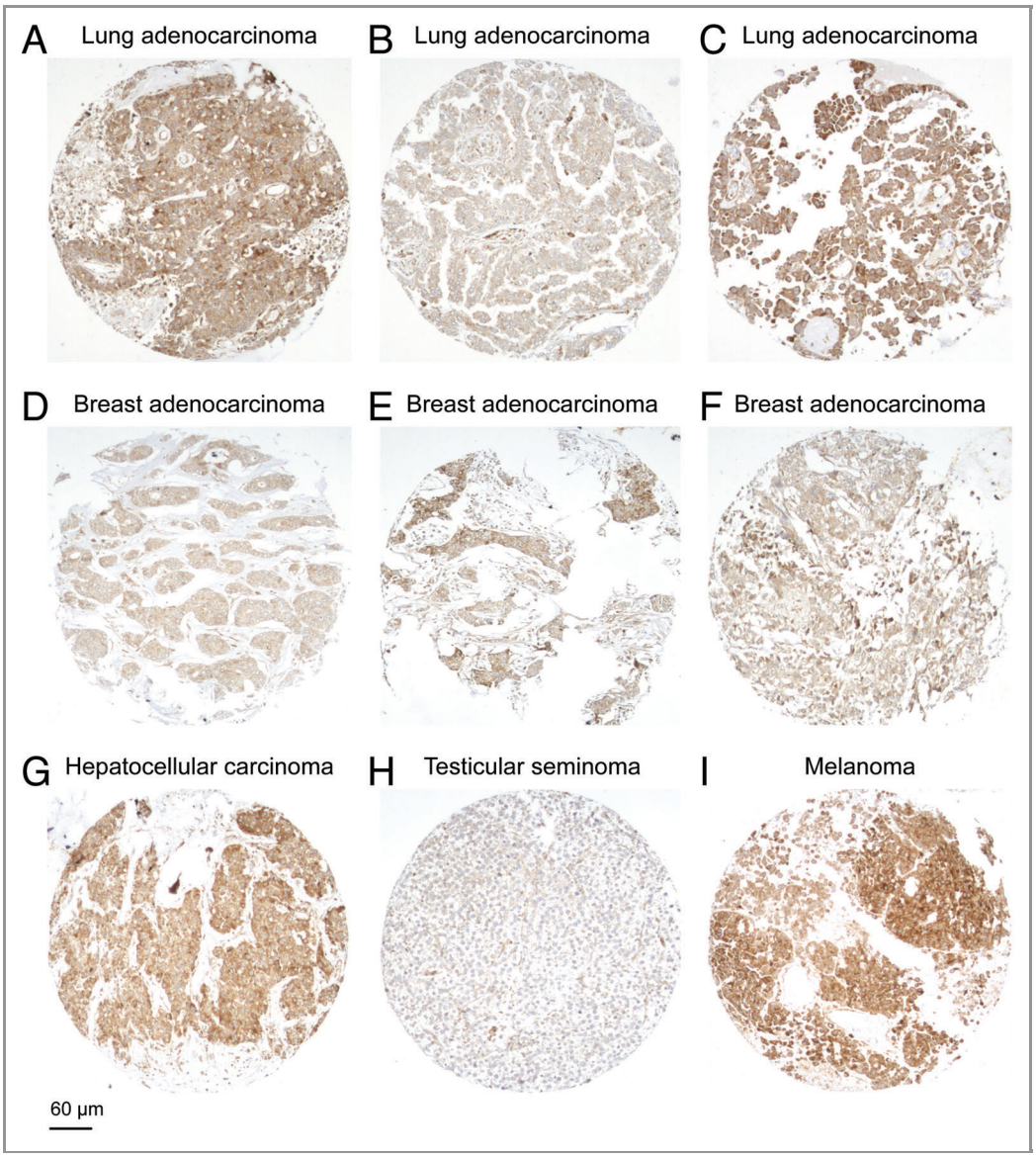

Figure 4. Representative LC3 staining patterns in malignant tissues. Tissue microarrays encompassing distinct neoplastic tissues were stained for the immunohistochemical detection of LC3, as detailed in Materials and Methods. Representative images are reported: (A–C) lung adenocarcinomas, (D–F) breast adenocarcinomas, (G) hepatocellular carcinoma, (H) testicular seminoma and (I) melanoma. Scale bar: 60 µm.

to establish similar protocols as the one described herein for the detection of additional LC3 isoforms or more distant members of the LC3 family (such as the γ-aminobutyric acid receptor-associated protein, GABARAP, and the Golgi-associated ATPase enhancer of 16 kDa, GATE-16).

Relatively little is known about autophagy levels in healthy (or at least nonmalignant) human tissues. In our study, many non-neoplastic cells, notably colon and placental cells, harbored a weak LC3 staining, confirming previous studies on these organs.[25-27] In kidneys, we observed a diffuse staining in the epithelial lining of tubules and glands, consistent with the physiological role of autophagy in renal function.[28] Although tumor cells tended to stain more intensely for LC3 than normal cells, it should be noted that normal immune cells, stromal fibroblasts or tumor infiltrating lymphocytes (TILs) could be strongly positive for LC3, rendering it difficult to distinguish normal stromal cells from cancer cells with a fibroblastoid or lymphoid morphology. Thus, LC3 immunostaining cannot be used as the sole criterion to distinguish malignant from non-malignant cells. As it was previously described for colorectal cancer,[26] we found that breast tumor cells tend to express higher LC3 levels than the adjacent, nonmalignant parenchyma. Moreover, LC3 puncta were generally absent from nontransformed breast epithelia. These staining patterns were comparable to those previously described in breast carcinoma.[29] However, the prognostic or predictive value of LC3 expression remains controversial[13,29,30] and requires further studies on large patient cohorts.

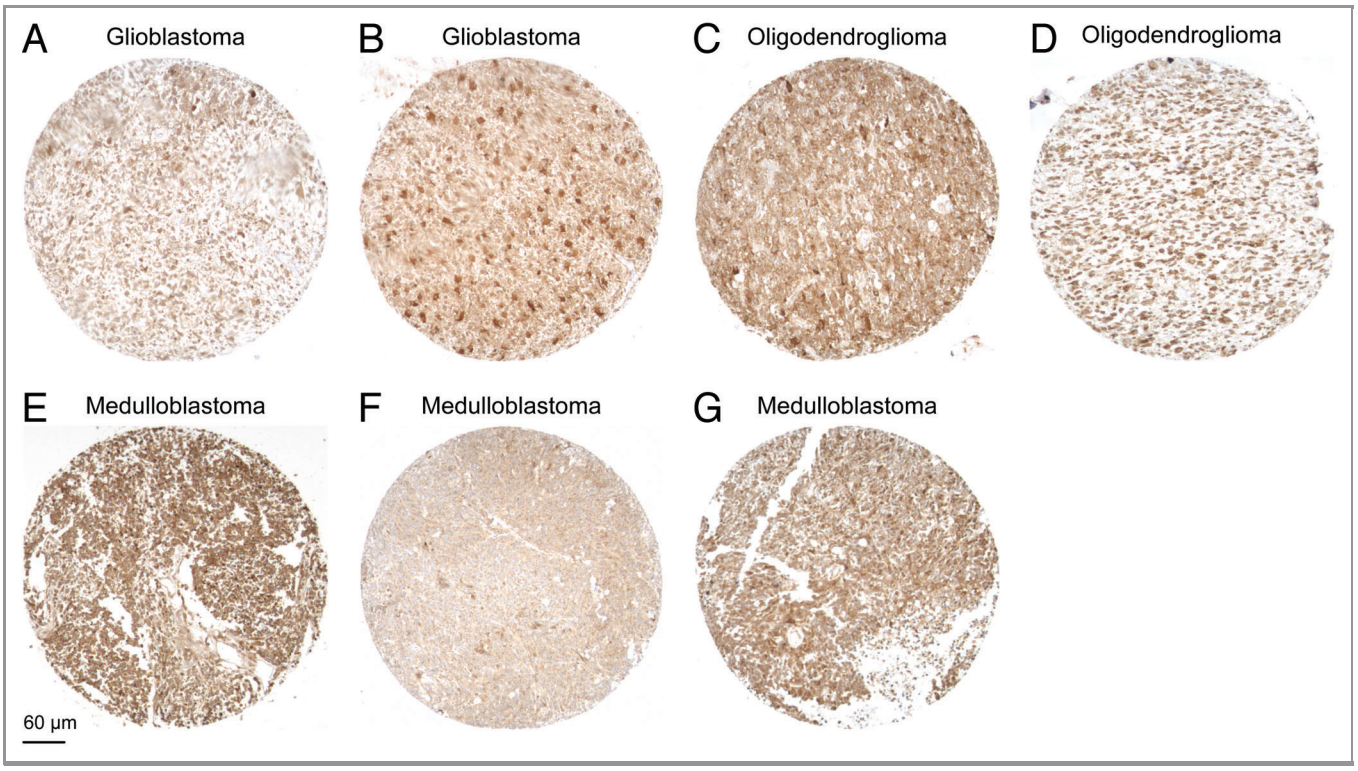

Figure 5. Representative LC3 staining patterns in CNS tumors. Tissue microarrays encompassing distinct CNS tumors were stained for the immunohistochemical detection of LC3, as detailed in Materials and Methods. Representative images are reported: (A and B) glioblastoma, (C and D) oligodendroglioma and (E–G) medulloblastoma. Scale bar: 60 μm.

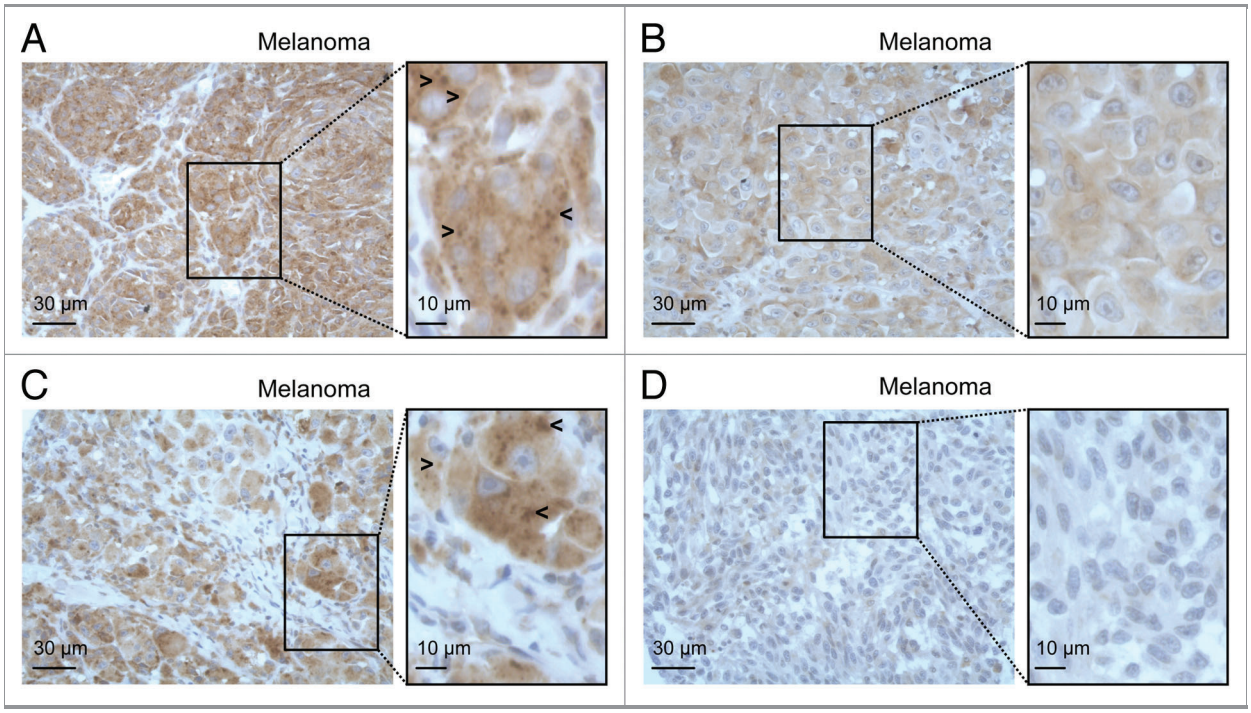

Figure 6. Representative LC3 staining patterns in melanoma. Tissue microarrays encompassing distinct melanoma samples were stained for the immunohistochemical detection of LC3, as detailed in Materials and Methods. Representative images are reported. Scale bars: 10 or 30 μm, as indicated.

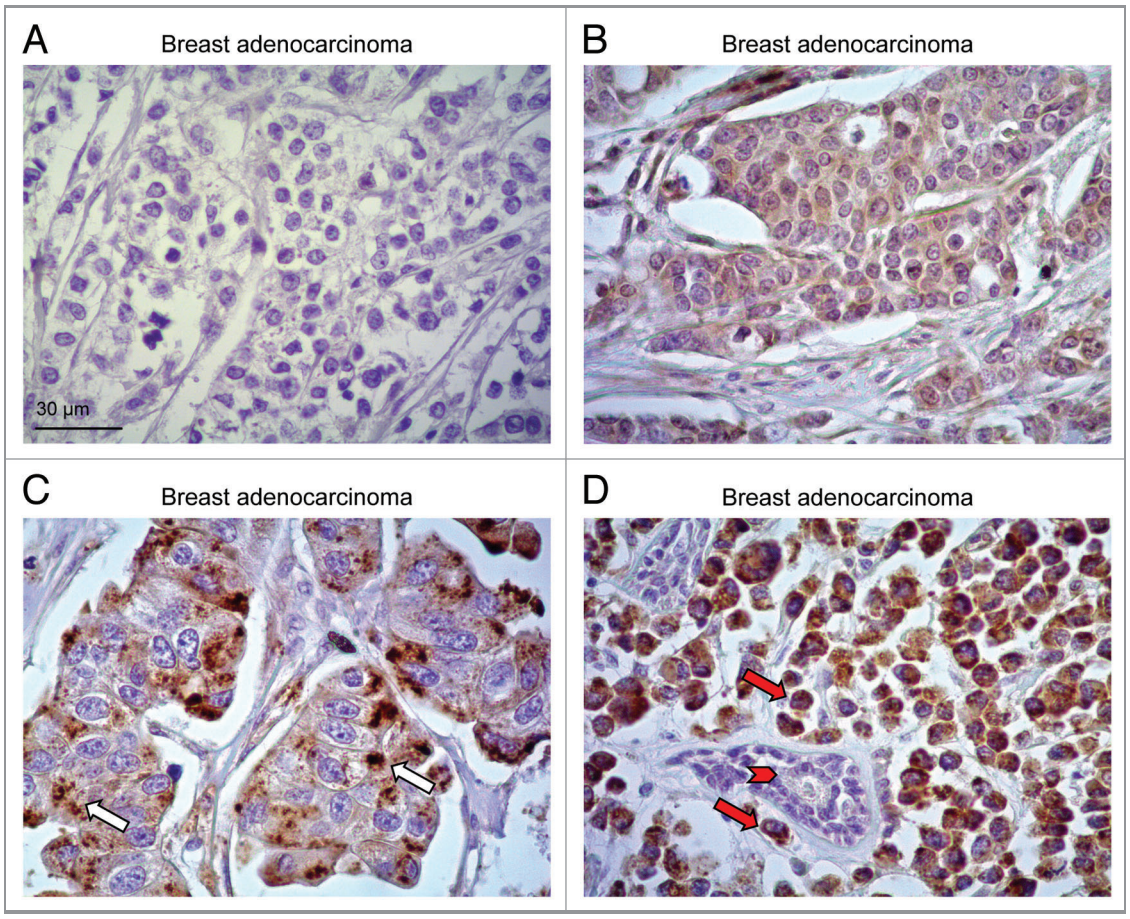

Figure 7. Representative LC3 staining patterns in breast adenocarcinoma: (A–D) breast adenocarcinoma tissues were stained for the immunohistochemical detection of LC3, as detailed in Materials and Methods. Representative staining patterns are reported: (A) absent expression, (B) diffuse cytoplasmic distribution, (C) LC3 puncta (white arrows) and (D) absent expression in normal breast cells (red arrowhead) + LC3 puncta in malignant cells (red arrows). Scale bar: 30 μm.

Materials and Methods

Chemicals, cell lines and culture conditions. Unless otherwise indicated, media, antibiotics and supplements for cell culture were purchased from Gibco-Invitrogen, plasticware from Corning Life Sciences, and chemicals from Sigma-Aldrich. Bafilomycin A_1 (1334) and rapamycin (1292) were purchased from Tocris, G418 sulfate (345810) from Calbiochem, puromycin (ant-pr-1) and zeocin (ant-zn-5) from Invivogen. Murine colon carcinoma CT26 cells (class I MHC haplotype H-2d, syngenic to BALB/c mice), murine fibrosarcoma MCA205 cells (class I MHC haplotype H-2b, syngenic for C57BL/6 mice) and their derivatives were cultured in RPMI 1640 medium supplemented with 10% heat-inactivated fetal bovine serum, 10 mM HEPES buffer, 10 U/mL penicillin sodium and 10 μg/mL streptomycin sulfate. CT26 cells stably expressing a green fluorescent protein (GFP)-LC3 chimera,[31] were maintained in the presence of 500 μg/mL G148.

To obtain autophagy-deficient CT26 and MCA205 cells, a set of plasmids encoding short-hairpin RNAs (shRNAs) specific for murine Atg5 (TR500113) and Atg7 (TR504956) plus a control shRNA were obtained from OriGene. These plasmids were used to generate control cells (SCR), as well as cells stably depleted of Atg5 ($Atg5^{KD}$) and Atg7 ($Atg7^{KD}$). $Atg5^{KD}$ or $Atg7^{KD}$ CT26 and MCA205 cells were maintained under 10 or 5 μg/mL puromycin selection, respectively.

Immunoblotting. Five × 10^5 cells were washed in PBS and subjected to lysis following established protocols.[32,33] Forty to 50 μg of proteins were separated according to molecular weight on NuPAGE Novex Bis-Tris 4–12% pre-cast gels (Invitrogen, NP0323BOX) and electrotransferred to PVDF membranes (Bio-Rad, 162-0177). Unspecific binding was blocked with 5% non-fat milk in 0.1% Tween20 for 1 h, followed by overnight incubation at 4°C with primary antibodies specific for the following proteins: β-actin (Millipore, MAB1501), ATG5 (Sigma-Aldrich, A0731), ATG7 (Sigma-Aldrich, A2856) and LC3B (Cell Signaling Technology, 2775). Primary antibodies were revealed with appropriate horseradish peroxidase-labeled conjugates (Southern Biotechnologies Associates, 4050-05 or 1031-05) and the SuperSignal West Pico chemoluminescent substrate (Thermo Fisher Scientific, PI-34078).

Immunofluorescence. Cells growing on coverslips were fixed in 4% PFA for 15 min at room temperature, and then permeabilized

with 0.1% TritonX-100 for 10 min.[34] Unspecific binding was blocked with 5% bovine serum in PBS, followed by staining with a primary antibody specific for LC3B (MBL International, M152-3) overnight at 4°C. Revelation was performed with an AlexaFluor®-488 conjugate (Molecular Probes-Invitrogen, A-11029). Nuclear counterstaining was obtained with 10 μM Hoechst 33342 (Molecular Probes-Invitrogen, H1399). Fluorescence microscopy images were acquired either on an LSM 510 microscope (Carl Zeiss) equipped with a DC300F camera or on a BD pathway 855 automated microscope (BD Imaging Systems) equipped with a 40× objective (Olympus) coupled to a robotized Twister II plate handler (Caliper Life Sciences). Images were analyzed for the presence of cytoplasmic GFP-LC3$^+$ or LC3$^+$ puncta by means of the BD Attovision software (BD Imaging Systems).

Immunohistochemical staining of human samples. Immunohistochemical staining of human cancer tissue sections was performed using the Novolink Kit (Menarini Diagnostics, RE7140-K). Briefly, 4 μm-thick formalin-fixed, paraffin-embedded tissue sections were deparaffinized with 3 successive passages through xylene, and rehydrated through decreasing concentrations (100%, 95%, 80%, 70% and 50%) of ethanol. Antigen retrieval was performed by heating slides for 30 min in pH 6.0 citrate buffer at 95°C. Slides were then allowed to cool at room temperature for 45 min, mounted on Shandon Sequenza coverplates (Thermo Fisher Scientific, 72-199-50) in distilled water, and then washed twice for 5 min with 0.1% Tween 20 (v/v in PBS). Thereafter, sections were incubated for 5 min with the Peroxidase Block reagent, and subsequently washed twice for 5 min with 0.1% Tween 20 (v/v in PBS). Following incubation for 5 min at room temperature with the Protein Block reagent, tissue sections were washed twice for 5 min with 0.1% Tween 20 (v/v in PBS), and then incubated overnight at 4°C with a primary antibody specific for LC3B (clone 5F10, from Nanotools, 0231-100), or with an isotype-matched IgG_1 (R&D Systems, MAB002), both dissolved in 1% bovine serum albumin (w/v in TBS) at the final concentration of 25 μg/mL. The 5F10 antibody recognizes both the soluble (LC3-I) and the membrane-bound form (LC3-II) of LC3B. After two washes in 0.1% Tween 20 (v/v in PBS), sections were incubated for 30 min with the Post Primary Block reagent, washed again as before and incubated for 30 min with the horseradish peroxidase-coupled Polymer secondary antibodies. Upon two additional washes, secondary antibodies were revealed with the liquid DAB Substrate Chromogen system (10 min incubation). Finally, slides were washed in distilled water, and counterstained with hematoxylin.

Immunohistochemical staining of mouse tissues and pelleted cells. Immunohistochemical staining of (murine) tissue sections and (human or murine) pelleted cells was performed as above, with minimal variations. In particular, slides were incubated for 20 min with the MOM Blocker IgG Mouse reagent (2%, v/v in 0.1% Tween 20 in PBS) after the passage in the Protein Block reagent, followed by 2 washes in 0.1% Tween 20 in PBS and incubation for 1 h with the anti-LC3 antibody (or with an isotype-matched IgG_1), used at the final concentration of 1 μg/mL.

Chemotherapy of established tumors in mice. Animals were maintained in specific pathogen-free conditions, and experiments followed the Federation of European Laboratory Animal Science Association (FELASA) guidelines. Animal experiments were approved by the local Ethics Committee (CEEA IRCIV / IGR n°26, registered with the French Ministry of Research) and were in compliance with the EU 63/2010 directive. Animals were used between 6 and 20 weeks of age and those bearing tumors exceeding 20–25% body mass were euthanatized. BALB/c (H-2d), C57BL/6 (H-2b) mice were obtained from Janvier or Harlan. BALB/c mice were subcutaneously inoculated with 5×10^5 SCR, Atg5^{KD} or Atg7^{KD} CT26 cells. C57BL/6 mice were inoculated with 2×10^5 SCR, Atg5^{KD} or Atg7^{KD} MCA205 cells. When tumor size reached 40–80 mm^2, mice were treated intraperitoneally with 5.17 mg/kg MTX in 200 μL sterile PBS.

Construction of tissue microarrays (TMAs). Formalin-fixed paraffin-embedded (FFPE) tissue blocks were retrieved from the archives of the Department of Pathology of the Institut Gustave Roussy (Villejuif, France). Hematoxylin/eosin-stained slides from each block were reviewed by a pathologist (FA) to identify tumor areas. TMAs were constructed with 0.6 mm diameter tissue cores from representative tumor areas from FFPE blocks. Cores were transferred to a paraffin block using a semi-automated tissue array instrument (Alphelys). Triplicate tissue cores were taken from each specimen, resulting in a composite TMA block containing cores from 31 different tumor specimens. Control tissues from lung, liver, placenta, colon, skin, thyroid, brain, lymph nodes and kidney were also included. Multiple 4 μm-thick sections were cut for hematoxylin and immunohistochemical staining.

Disclosure of Potential Conflicts of Interest

No potential conflicts of interest were disclosed.

Acknowledgments

GK is supported by the Ligue Nationale contre le Cancer (Equipes labelisée), Agence Nationale pour la Recherche (ANR), European Commission (Active p53, Apo-Sys, ChemoRes, ApopTrain), Fondation pour la Recherche Médicale (FRM), Institut National du Cancer (INCa), Cancéropôle Ile-de-France, Fondation AXA, Fondation Bettencourt-Schueller and the LabEx Immuno-Oncology. M.M. is supported by Fondation AXA. I.M. and S.A. are supported by the Ligue Nationale contre le Cancer. L.G. is funded by the LabEx Immuno-Oncology.

Supplemental Materials

Supplemental materials may be found here:
www.landesbioscience.com/journals/autophagy/article/20353

References

1. De Duve C, Wattiaux R. Functions of lysosomes. Annu Rev Physiol 1966; 28:435-92; PMID:5322983; http://dx.doi.org/10.1146/annurev.ph.28.030166.002251
2. Klionsky DJ. Autophagy: from phenomenology to molecular understanding in less than a decade. Nat Rev Mol Cell Biol 2007; 8:931-7; PMID:17712358; http://dx.doi.org/10.1038/nrm2245
3. Green DR, Galluzzi L, Kroemer G. Mitochondria and the autophagy-inflammation-cell death axis in organismal aging. Science 2011; 333:1109-12; PMID:21868666; http://dx.doi.org/10.1126/science.1201940
4. Reggiori F, Klionsky DJ. Autophagosomes: biogenesis from scratch? Curr Opin Cell Biol 2005; 17:415-22; PMID:15978794; http://dx.doi.org/10.1016/j.ceb.2005.06.007
5. Rosenfeldt MT, Ryan KM. The role of autophagy in tumour development and cancer therapy. Expert Rev Mol Med 2009; 11:e36; PMID:19951459; http://dx.doi.org/10.1017/S1462399409001306
6. Yu L, McPhee CK, Zheng L, Mardones GA, Rong Y, Peng J, et al. Termination of autophagy and reformation of lysosomes regulated by mTOR. Nature 2010; 465:942-6; PMID:20526321; http://dx.doi.org/10.1038/nature09076
7. Klionsky DJ, Abeliovich H, Agostinis P, Agrawal DK, Aliev G, Askew DS, et al. Guidelines for the use and interpretation of assays for monitoring autophagy in higher eukaryotes. Autophagy 2008; 4:151-75; PMID:18188003
8. Kabeya Y, Mizushima N, Ueno T, Yamamoto A, Kirisako T, Noda T, et al. LC3, a mammalian homologue of yeast Apg8p, is localized in autophagosome membranes after processing. EMBO J 2000; 19:5720-8; PMID:11060023; http://dx.doi.org/10.1093/emboj/19.21.5720
9. Kabeya Y, Mizushima N, Yamamoto A, Oshitani-Okamoto S, Ohsumi Y, Yoshimori T. LC3, GABARAP and GATE16 localize to autophagosomal membrane depending on form-II formation. J Cell Sci 2004; 117:2805-12; PMID:15169837; http://dx.doi.org/10.1242/jcs.01131
10. Mizushima N, Levine B, Cuervo AM, Klionsky DJ. Autophagy fights disease through cellular self-digestion. Nature 2008; 451:1069-75; PMID:18305538; http://dx.doi.org/10.1038/nature06639
11. Rosenfeldt MT, Ryan KM. The multiple roles of autophagy in cancer. Carcinogenesis 2011; 32:955-63; PMID:21317301; http://dx.doi.org/10.1093/carcin/bgr031
12. Chen Y, Azad MB, Gibson SB. Methods for detecting autophagy and determining autophagy-induced cell death. Can J Physiol Pharmacol 2010; 88:285-95; PMID:20393593; http://dx.doi.org/10.1139/Y10-010
13. Michaud M, Martins I, Sukkurwala AQ, Adjemian S, Ma Y, Pellegatti P, et al. Autophagy-dependent anticancer immune responses induced by chemotherapeutic agents in mice. Science 2011; 334:1573-7; PMID:22174255; http://dx.doi.org/10.1126/science.1208347
14. de Chastellier C. EM analysis of phagosomes. Methods Mol Biol 2008; 445:261-85; PMID:18425456; http://dx.doi.org/10.1007/978-1-59745-157-4_17
15. Kalamidas SA, Kondomerkos DJ, Kotoulas OB, Hann AC. Electron microscopic and biochemical study of the effects of rapamycin on glycogen autophagy in the newborn rat liver. Microsc Res Tech 2004; 63:215-9; PMID:14988919; http://dx.doi.org/10.1002/jemt.20032
16. Mizushima N, Yamamoto A, Hatano M, Kobayashi Y, Kabeya Y, Suzuki K, et al. Dissection of autophagosome formation using Apg5-deficient mouse embryonic stem cells. J Cell Biol 2001; 152:657-68; PMID:11266458; http://dx.doi.org/10.1083/jcb.152.4.657
17. Chen Y, McMillan-Ward E, Kong J, Israels SJ, Gibson SB. Mitochondrial electron-transport-chain inhibitors of complexes I and II induce autophagic cell death mediated by reactive oxygen species. J Cell Sci 2007; 120:4155-66; PMID:18032788; http://dx.doi.org/10.1242/jcs.011163
18. Tasdemir E, Galluzzi L, Maiuri MC, Criollo A, Vitale I, Hangen E, et al. Methods for assessing autophagy and autophagic cell death. Methods Mol Biol 2008; 445:29-76; PMID:18425442; http://dx.doi.org/10.1007/978-1-59745-157-4_3
19. Yang S, Wang X, Contino G, Liesa M, Sahin E, Ying H, et al. Pancreatic cancers require autophagy for tumor growth. Genes Dev 2011; 25:717-29; PMID:21406549; http://dx.doi.org/10.1101/gad.2016111
20. Guo JY, Chen HY, Mathew R, Fan J, Strohecker AM, Karsli-Uzunbas G, et al. Activated Ras requires autophagy to maintain oxidative metabolism and tumorigenesis. Genes Dev 2011; 25:460-70; PMID:21317241; http://dx.doi.org/10.1101/gad.2016311
21. Carew JS, Nawrocki ST, Kahue CN, Zhang H, Yang C, Chung L, et al. Targeting autophagy augments the anticancer activity of the histone deacetylase inhibitor SAHA to overcome Bcr-Abl-mediated drug resistance. Blood 2007; 110:313-22; PMID:17363733; http://dx.doi.org/10.1182/blood-2006-10-050260
22. Katayama M, Kawaguchi T, Berger MS, Pieper RO. DNA damaging agent-induced autophagy produces a cytoprotective adenosine triphosphate surge in malignant glioma cells. Cell Death Differ 2007; 14:548-58; PMID:16946731; http://dx.doi.org/10.1038/sj.cdd.4402030
23. Tanida I, Waguri S. Measurement of autophagy in cells and tissues. Methods Mol Biol 2010; 648:193-214; PMID:20700714; http://dx.doi.org/10.1007/978-1-60761-756-3_13
24. Tanida I. Autophagy basics. Microbiol Immunol 2011; 55:1-11; PMID:21175768; http://dx.doi.org/10.1111/j.1348-0421.2010.00271.x
25. Signorelli P, Avagliano L, Virgili E, Gagliostro V, Doi P, Braidotti P, et al. Autophagy in term normal human placentas. Placenta 2011; 32:482-5; PMID:21459442; http://dx.doi.org/10.1016/j.placenta.2011.03.005
26. Sato K, Tsuchihara K, Fujii S, Sugiyama M, Goya T, Atomi Y, et al. Autophagy is activated in colorectal cancer cells and contributes to the tolerance to nutrient deprivation. Cancer Res 2007; 67:9677-84; PMID:17942897; http://dx.doi.org/10.1158/0008-5472.CAN-07-1462
27. Guo GF, Jiang WQ, Zhang B, Cai YC, Xu RH, Chen XX, et al. Autophagy-related proteins Beclin-1 and LC3 predict cetuximab efficacy in advanced colorectal cancer. World J Gastroenterol 2011; 17:4779-86; PMID:22147978; http://dx.doi.org/10.3748/wjg.v17.i43.4779
28. Isaka Y, Kimura T, Takabatake Y. The protective role of autophagy against aging and acute ischemic injury in kidney proximal tubular cells. Autophagy 2011; 7:1085-7; PMID:21606682; http://dx.doi.org/10.4161/auto.7.9.16465
29. Sivridis E, Koukourakis MI, Zois CE, Ledaki I, Ferguson DJ, Harris AL, et al. LC3A-positive light microscopy detected patterns of autophagy and prognosis in operable breast carcinomas. Am J Pathol 2010; 176:2477-89; PMID:20382705; http://dx.doi.org/10.2353/ajpath.2010.090049
30. Lazova R, Camp RL, Klump V, Siddiqui SF, Amaravadi RK, Pawelek JM. Punctate LC3B expression is a common feature of solid tumors and associated with proliferation, metastasis, and poor outcome. Clin Cancer Res 2012; 18:370-9; PMID:22080440; http://dx.doi.org/10.1158/1078-0432.CCR-11-1282
31. Shen S, Kepp O, Michaud M, Martins I, Minoux H, Métivier D, et al. Association and dissociation of autophagy, apoptosis and necrosis by systematic chemical study. Oncogene 2011; 30:4544-56; PMID:21577201; http://dx.doi.org/10.1038/onc.2011.168
32. Criollo A, Galluzzi L, Maiuri MC, Tasdemir E, Lavandero S, Kroemer G. Mitochondrial control of cell death induced by hyperosmotic stress. Apoptosis 2007; 12:3-18; PMID:17080328; http://dx.doi.org/10.1007/s10495-006-0328-x
33. Galluzzi L, Morselli E, Vitale I, Kepp O, Senovilla L, Criollo A, et al. miR-181a and miR-630 regulate cisplatin-induced cancer cell death. Cancer Res 2010; 70:1793-803; PMID:20145152; http://dx.doi.org/10.1158/0008-5472.CAN-09-3112
34. Boehrer S, Adès L, Braun T, Galluzzi L, Grosjean J, Fabre C, et al. Erlotinib exhibits antineoplastic off-target effects in AML and MDS: a preclinical study. Blood 2008; 111:2170-80; PMID:17925489; http://dx.doi.org/10.1182/blood-2007-07-100362